Biochemistry

Article

Cite This: *Biochemistry* 2019, 58, 1751−1763

pubs.acs.org/biochemistry

Mechanism of 6-Hydroxynicotinate 3-Monooxygenase, a Flavin-Dependent Decarboxylative Hydroxylase Involved in Bacterial Nicotinic Acid Degradation

Kent D. Nakamoto,[†] Scott W. Perkins,[†] Ryan G. Campbell,[†] Matthew R. Bauerle,[†] Tyler J. Gerwig,[†] Selim Gerislioglu,[‡] Chrys Wesdemiotis,[‡] Mark A. Anderson,[§] Katherine A. Hicks,[∥] and Mark J. Snider*[,†]

[†]Department of Chemistry, The College of Wooster, Wooster, Ohio 44691, United States

[‡]Department of Chemistry, University of Akron, Akron, Ohio 44325, United States

[§]Institute for Enzyme Research, Department of Biochemistry, University of Wisconsin, Madison, Wisconsin 53726, United States

[∥]Department of Chemistry, The State University of New York College at Cortland, Cortland, New York 13045, United States

Supporting Information

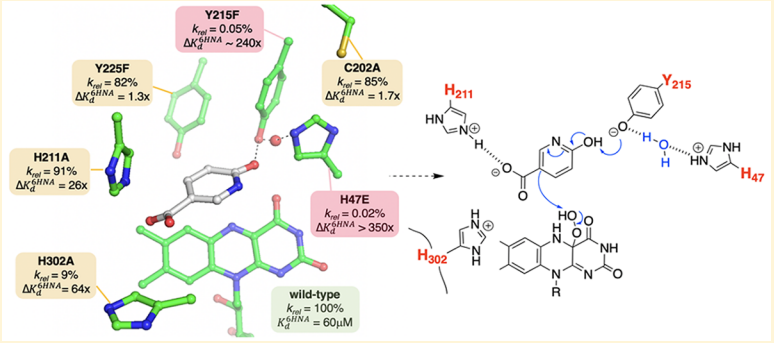

ABSTRACT: 6-Hydroxynicotinate 3-monooxygenase (NicC) is a Group A FAD-dependent monooxygenase that catalyzes the decarboxylative hydroxylation of 6-hydroxynicotinic acid (6-HNA) to 2,5-dihydroxypyridine (2,5-DHP) with concomitant oxidation of NADH in nicotinic acid degradation by aerobic bacteria. Two mechanisms for the decarboxylative hydroxylation half-reaction have been proposed [Hicks, K., et al. (2016) *Biochemistry* 55, 3432−3446]. Results with *Bordetella bronchiseptica* RB50 NicC here show that a homocyclic analogue of 6-HNA, 4-hydroxybenzoic acid (4-HBA), is decarboxylated and hydroxylated by NicC with a 420-fold lower catalytic efficiency than is 6-HNA. The $^{13}(V/K)$, measured with wild-type NicC by isotope ratio mass spectrometry following the natural abundance of ^{13}C in the CO_2 product, is inverse for both 6-HNA (0.9989 ± 0.0002) and 4-HBA (0.9942 ± 0.0004) and becomes negligible (0.9999 ± 0.0004) for 5-chloro-6-HNA, an analogue that is 10-fold more catalytically efficient than 6-HNA. Covalently bound 6-HNA complexes of NicC are not observed by mass spectrometry. Comparative steady-state kinetic and K_d^{6HNA} analyses of active site NicC variants (C202A, H211A, H302A, H47E, Y215F, and Y225F) identify Tyr215 and His47 as critical determinants both of 6-HNA binding (K_d^{Y215F}/K_d^{WT} > 240; K_d^{H47E}/K_d^{WT} > 350) and in coupling rates of 2,5-DHP and NAD^+ product formation ([2,5-DHP]/[NAD^+] = 1.00 (WT), 0.005 (Y215F), and 0.07 (H47E)]. Results of these functional analyses are in accord with an electrophilic aromatic substitution reaction mechanism in which His47−Tyr215 may serve as the general base to catalyze substrate hydroxylation and refine the structural model for substrate binding by NicC.

The enzymology of nicotinic acid (NA) catabolism is a useful model system for understanding the biochemical mechanisms that have evolved that allow bacteria to degrade N-heterocyclic aromatic compounds (NHACs), a class of molecules that are found in the environment from natural and ubiquitous anthropogenic sources.[1−3] NHACs including nicotine, pyridine, indole, and quinoline are toxic[4] but also serve as biomass and energy sources for bacteria.[5,6] NHAC biodegradation begins by the hydroxylation of the N-heteroaromatic ring,[7] catalyzed by dehydrogenases and monooxygenases. More detailed knowledge concerning the bacterial mechanisms of NHAC catabolism, particularly the hydroxylation steps that serve to activate the ring for cleavage, may lead to optimized bioremediation strategies.

The first hydroxylation of NA, catalyzed by a multisubunit, Mo-dependent dehydrogenase complex, uses water as the

Received: September 10, 2018
Revised: February 25, 2019
Published: February 27, 2019

DOI: 10.1021/acs.biochem.8b00969
Biochemistry 2019, 58, 1751−1763

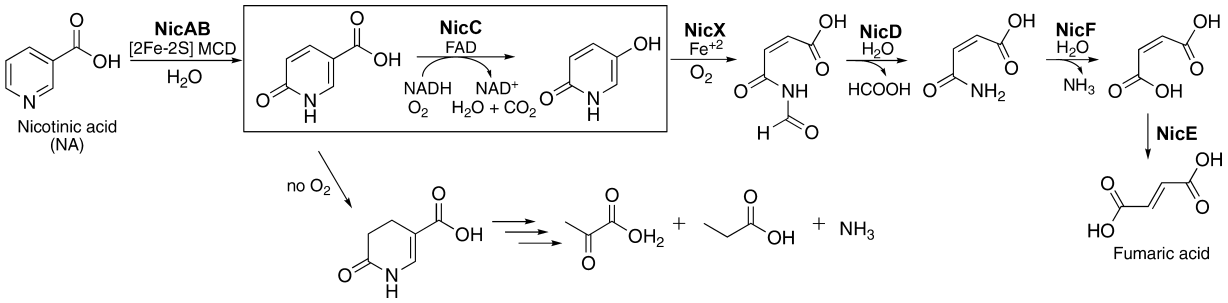

Figure 1. Nicotinic acid (NA) degradation pathway in aerobic bacteria (e.g., *Pseudomonas putida* KT2440 and *Bordetella bronchiseptica* RB50) and an abbreviated pathway in anaerobic bacteria (e.g., *Eubacterium barkeri*). 6-HNA serves as a key intermediate in both pathways. The reaction catalyzed by flavin-dependent 6-hydroxynicotinate 3-monooxygenase (NicC) is boxed.

source of oxygen and generates 6-hydroxynicotinic acid (6-HNA),[8] a common intermediate in all known NA degradation pathways (Figure 1).[9−12] Subsequent transformations of 6-HNA are dependent on the species of bacteria. In multiple aerobic bacteria, 6-HNA undergoes a decarboxylative hydroxylation catalyzed by the flavin-dependent 6-hydroxynicotinate 3-monooxygenase (NicC; UniProtKB entry A0A0H3LKL4).

NicC is part of the Group A flavin monooxygenases (FMOs), a class of enzymes that catalyze multistep reaction mechanisms involving the reduction of FAD using NADH, the activation of O_2 by forming a reactive C(4a)-hydroperoxy flavin intermediate, and subsequent hydroxylation of its organic substrate.[13,14] NicC is relatively unique among the enzymes of this class in that it catalyzes the removal of CO_2 and addition of -OH on the same carbon (C3) within a pyridine ring. Of the known decarboxylative hydroxylation reactions using aromatic substrates catalyzed by Group A FMOs (Figure S1), only three involve pyridine ring (N-heterocyclic) substrates, and among these, the reactions of hydroxylation and C−C bond cleavage have distinctions. For instance, the C−C cleavage reaction catalyzed by 6-hydroxy-3-succinoylpyridine 3-monooxygenase (HspB, UniProtKB entry F8G0M4) releases succinate and not CO_2. Likewise, it is interesting to note that the members of Group A FMOs have low sequence identities (for example, those FMOs with >50% sequence coverage of NicC have only 29−36% sequence identity). These observations suggest that the mechanisms of catalysis of decarboxylative hydroxylations by these FMOs may have unique characteristics. Given the common strategies for NHAC biodegradation, it is worth noting that Group A FMOs have been identified as potentially important bioengineering targets for catalysis of regioselective hydroxylation of pharmaceuticals and fine chemicals.[15] Thus, a better understanding of the mechanisms and diverse active site architectures within this class of enzymes is of general interest.

We recently reported[16] the crystal structure of the flavin-bound NicC enzyme from *Pseudomonas putida* KT2440 [Protein Data Bank (PDB) entry 5EOW] (Figure 2) and offered two potential mechanisms (Figure 3) for the decarboxylative hydroxylation of 6-HNA to 2,5-dihydroxypyridine (2,5-DHP) involving the C(4a)-hydroperoxy flavin intermediate. The mechanistic proposal that is colored blue, involving the covalent addition of an active site thiolate to 6-HNA, uses the more stable keto tautomer of 6-HNA, possible only in pyridine ring substrates, to serve as an initial electron sink. Subsequent electron rearrangement from the phenolic oxyanion intermediate would enable hydroxylation. Direct abstraction of the 6-OH from the enol tautomer of 6-HNA, illustrated in the mechanistic proposal that is colored red,

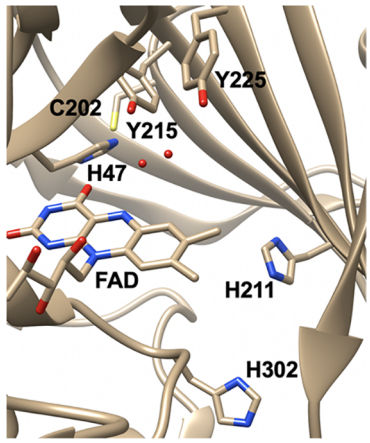

Figure 2. Ribbon diagram of the active site of NicC (PDB entry 5EOW).[16] Putative active site residues and the FAD cofactor are shown as sticks and colored according to atom type. This figure was produced using the UCSF Chimera package from the Resource for Biocomputing, Visualization, and Informatics at the University of California, San Francisco (supported by National Institutes of Health Grant P41 RR-01081).

promotes hydroxylation at C3. In both mechanisms, subsequent decarboxylation of the resulting tetrahedral intermediate at C3 enables rearomatization to form the final product, 2,5-dihydroxypyridine (2,5 DHP). The mechanistic proposal that is colored red is commonly accepted for the FMOs that catalyze this reaction with substituted homocyclic rings where the organic substrate is the phenol. To discern whether either of these mechanisms is possible for NicC and the active site determinants of substrate binding and catalysis, we measured the kinetic and equilibrium binding properties of NicC with alternative substrates and likewise with active site variants of NicC. Because Group A FMO-catalyzed reactions require precise orchestration of NADH oxidation, O_2 activation, and substrate hydroxylation, they have evolved dynamic active sites that couple these reactions to prevent wasteful depletion of cellular NADH levels, and in some cases, the mechanism of product coupling has been well-defined (see, for example, ref 17). Thus, upon comparison of the rates of active site variants, it was important to determine whether the rate of formation of the products, NAD^+ and 2,5-DHP, retains the same stoichiometric ratio as observed for wild-type NicC. Because H_2O_2 can dissociate from the C(4a)-hydroperoxy flavin, variants with increased activation energies for transferring the hydroxyl moiety to 6-HNA may turn over by this alternative "uncoupled" pathway (Figure 4). The observed loss of product coupling,

DOI: 10.1021/acs.biochem.8b00969
Biochemistry 2019, 58, 1751−1763

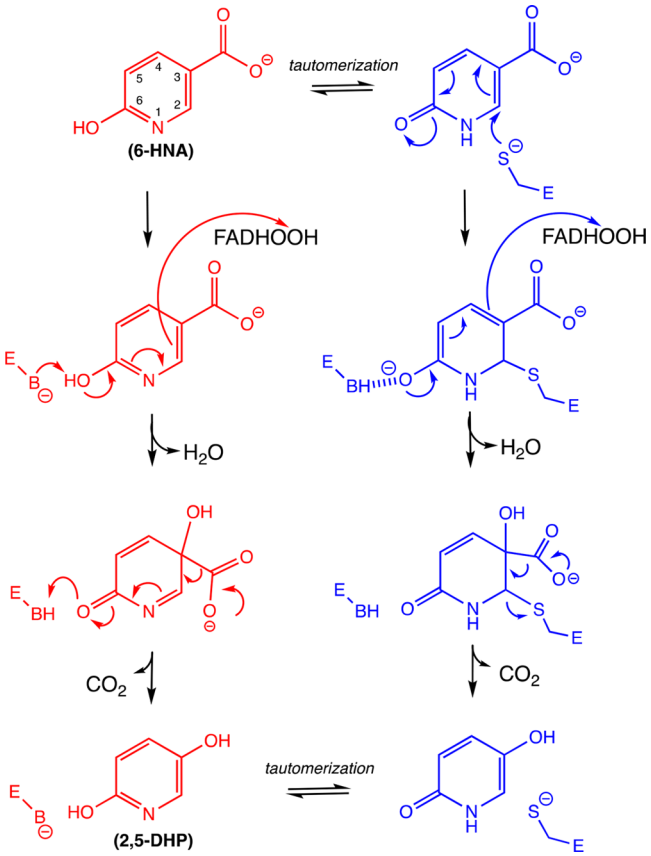

Figure 3. Two mechanistic proposals for the substrate hydroxylation and decarboxylation reaction catalyzed by NicC using the C(4a)-hydroperoxyflavin intermediate (FADHOOH). The proposal that is colored blue uses the 6-oxo tautomer of the substrate and involves Michael addition of a thiolate to generate an oxyanion intermediate that subsequently initiates hydroxylation. The proposal that is colored red illustrates the deprotonation of the 6-enol tautomer by an active site general base that initiates hydroxylation. Decarboxylation of the resulting tetrahedral intermediate in each rearomatizes the ring and forms 2,5-DHP.

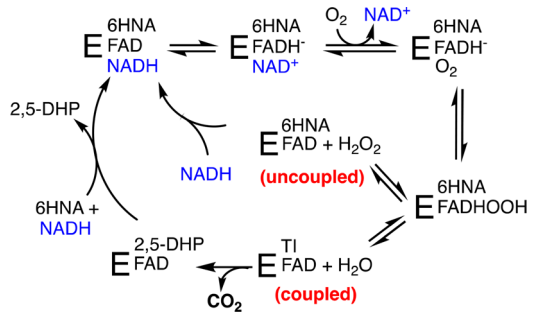

Figure 4. Simplified schematic representation of the NicC-catalyzed reaction showing the potential pathways for NADH oxidation and either productive (coupled) formation of 2,5-dihydroxypyridine or uncoupled reactions resulting in hydrogen peroxide formation. TI represents the tetrahedral intermediate, in which -OH and -CO_2 are both attached at C3 of the pyridine ring.

therefore, provides additional evidence of whether an active site residue may be involved in the catalytic steps involving substrate hydroxylation.

MATERIALS AND METHODS

Site-Directed Mutagenesis. The molecular cloning of the *Bb*1770 gene (encoding NicC) from *Bordetella bronchiseptica* RB50 into a pET-28-based *Escherichia coli* expression plasmid (pTHT) has been described.[16] The polymerase chain reaction (PCR)-based engineering of the C202A, Y215F, Y225F, H211A, H302A, H47A, H47F, and H47E variants of NicC was achieved using the Q5 Site-Directed Mutagenesis Kit (New England Biolabs, Ipswich, MA). A list of mutagenesis primers (purchased from IDT, Inc., Skokie, IL) is provided (Table S1). DNA sequencing of the entire gene confirmed the successful creation of each point mutation. The numbering of the primary sequence is based on that of *P. putida* NicC.

***Bb*NicC Expression and Purification.** Recombinant wild-type and variant *Bb*NicC enzymes were overproduced in BL21 (DE3) cells (Novagen) and purified using nickel ion affinity chromatography (HisTrap HP columns, GE Life Sciences) as reported previously.[16] Each variant was purified using a new HisTrap HP column, and the FPLC instrument washed with 1.0 M NaOH between applications. Protein purity was confirmed by sodium dodecyl sulfate−polyacrylamide gel electrophoresis analysis. After concentration by centrifugation (YM-10 Amicon ultrafiltration 10 kDa), each enzyme stock was exchanged into storage buffer [Tris (10 mM, pH 7.2), NaCl (100 mM), glycerol (25%, v/v), EDTA (0.1 mM), and DTT (2 mM)] using a 10DG column (Bio-Rad), flash-frozen in liquid N_2, and stored as aliquots at −80 °C. Prior to functional analysis, enzyme stocks were incubated with excess FAD overnight at 4 °C and then exchanged into reaction buffer [typically 50 mM phosphate buffer (pH 7.5)] to remove storage buffer and excess FAD. FAD-bound (active) enzyme concentrations were determined by absorbance (ε_{450} = 11900 ± 110 M^{-1} cm^{-1}) as previously described.[16]

^{13}C Kinetic Isotope Effects. Because a direct product of the NicC-catalyzed reaction is CO_2, a "one-pot" methodology was developed to prevent any exogenous CO_2 from entering the system. First, a saturated solution of NaOH was made in a sealed container with a septum and allowed to sit for 10 days to allow carbonate to precipitate before use. Separate solutions of NADH (100 mM in water) and 6-HNA [5.0 mM in Tricine (10 mM, pH 7.5), and then adjusted to pH 5 by addition (168 μL) of 4 N H_2SO_4] were sealed in glass flasks equipped with a side arm, a glass stopcock, and a septum. The flask containing the solution of 6-HNA was attached to a vacuum manifold and sparged (2 h) with dry, CO_2-free O_2. The flask containing the solution of NADH was sparged (2 h) with dry, CO_2-free N_2. After sparging, the solution of NADH (1.0 mL) and saturated NaOH (35 μL, to pH 8.4) were added to the 6-HNA solution (9.0 mL) via a gastight syringe. The reaction was then initiated by addition of wild-type NicC (100 μL; C_F ~ 100 nM). A small aliquot (10 μL) of the reaction mixture was removed periodically to determine the extent of reaction by absorbance at 360 nm ($\Delta\varepsilon$ = 3808 M^{-1} cm^{-1}). The reaction was observed to be 40% complete in approximately 3 h. To achieve complete (~100%) reactions, to determine the R_o values, additional enzyme was added (C_F ~ 225 nM) and the reaction mixtures were stirred at 25 °C for 15−18 h.

To remove undesired gases from the solution, the flasks were attached to a high-vacuum line, frozen at −78 °C, and subjected to two freeze−pump−thaw cycles. The degassed solution was then thawed, acidified with H_2SO_4 (4 N, 300 μL) to pH ~1.5, and stirred vigorously to release the CO_2. The mixture was

DOI: 10.1021/acs.biochem.8b00969
Biochemistry 2019, 58, 1751−1763

refrozen, and the CO_2 was distilled through two −78 °C traps and then isolated at −196 °C. Each CO_2 sample was measured individually by isotope ratio mass spectrometry to determine its isotopic ratio compared to a known standard to give a δ value defined as

$$\delta = 1000\left(\frac{^{13}C_{sample}/^{12}C_{sample}}{^{13}C_{standard}/^{12}C_{standard}} - 1\right) \quad (1)$$

The samples were then converted to an R value defined as

$$R_p = \frac{\delta_{sample}}{1000} + 1 \quad (2)$$

The R_p value was used in the following equation to obtain the isotope effect (IE):

$$IE = \frac{\ln(1-f)}{\ln\left[(1-f)^{\frac{R_p}{R_o}}\right]} \quad (3)$$

where f is the fraction of the reaction and R_o is the natural abundance isotopic ratio ($^{13}C/^{12}C$) in the starting material (determined experimentally from reactions run to completion).

Mass Spectrometry. Wild-type NicC (0.5 mg/mL) was incubated for 2−4 h in ammonium bicarbonate buffer (50 mM, pH 7.5) at room temperature with only 6-HNA (500 μM), with both NAD^+ (200 μM) and 6-HNA (500 μM), or without a substrate. Each sample was diluted to 0.01 mg/mL in an acetonitrile/H_2O/formic acid mixture [50:49.9:0.1 (v/v/v) MeCN:H_2O:FA] immediately prior to mass spectrometry (MS) analysis. All MS analysis was carried out by a Waters Synapt HDMS quadrupole/time-of-flight (Q/ToF) mass spectrometer (Waters, Milford, MA), equipped with an electrospray ionization (ESI) source. The diluted samples were injected into the ESI source by using an automated syringe pump at a flow rate of 20 μL/min. The ESI source parameters were adjusted as follows: capillary voltage, 3.1 kV; sampling cone voltage, 40 V; extraction cone voltage, 3.0 V; ion source temperature, 80 °C; desolvation temperature, 250 °C; and desolvation gas (N_2) flow rate, 600 L/h. The data were analyzed using Waters' MassLynx version 4.1 and deconvoluted using the MaxEnt 1 function in Waters' MassLynx version 4.1.

Continuous Kinetic Analysis of NADH Oxidation. Steady-state kinetic analyses of the NicC activity in sodium phosphate buffer (50 mM, pH 7.5, 25 °C) were performed by measuring changes in absorbance at 360 nm as previously described.[16] Briefly, the concentrations of both 6-HNA (50−2000 μM) and NADH (25−250 μM) were systematically varied, with a constant concentration of NicC (typically 50−100 nM). Stock solutions of 6-HNA were prepared in 50 mM sodium phosphate buffer (pH 7.5) prepared fresh every 1−3 days, and the stock concentration was determined by absorbance (ε_{295} = 5700 M^{-1} cm^{-1}). A global fit of the initial rate data using nonlinear regression analysis to the sequential ternary kinetic model (eq 4) was accomplished with GraFit version 5 [Leatherbarrow, R. J. (2007) *GraFit*, version 5, Erithacas Software Ltd., Horley, U.K.]:

$$v = (k_{cat}[E][NADH][6HNA])/(K_{ia}^{6HNA}K_M^{NADH} + K_M^{NADH}[6HNA] + K_M^{6HNA}[NADH] + [6HNA][NADH]) \quad (4)$$

Kinetic Analysis of 2,5-DHP and NAD^+ Formation and Coupling. Reaction mixtures (5 mL) containing 6-HNA (1−5 mM), NADH (200 μM or 1 mM), and NicC (25−500 nM) in potassium phosphate buffer (50 mM, pH 7.5) were incubated at 25 °C. The concentration of the NicC variant (C202A, H211A, H301A, H47E, Y215F, or Y225F) in each assay was adjusted on the basis of the variants' rate of NADH oxidation monitored at 360 nm. Aliquots were quenched at specific timed intervals, following the HPLC sample preparation detailed below, to separate and determine the concentrations of the NAD^+ and 2,5-DHP products.

pH Dependence of the Initial Rate of 2,5-DHP Formation. Reaction mixtures (5 mL) contained 6-HNA (2 mM) and NADH (1 mM) in a mixed buffer system [containing MES, HEPES, TAPS, and CAPS (50 mM each) and titrated with NaOH to a specific pH between 6.1 and 10.0] to maintain a consistent ionic strength. The reaction was initiated by addition of wild-type NicC or Y215F NicC variant (final concentration of 25 or 200 nM, respectively), and aliquots were removed and quenched in 4 min intervals over a reaction time of 20 min. Formation of the product was quantified following the HPLC sample preparation detailed below. Linear regression analysis of the change in 2,5-DHP concentration with time was used to determine the initial rate and the apparent steady-state rate constant (k_{OH}) at each pH. The pH dependence of k_{OH} was fit with a double-bell model (eq 5), using KaleidaGraph (version 4.1.3):

$$k_{obs} = \frac{k_{max}}{\frac{[H^+]}{K_{a1}} + \frac{K_{a1}}{[H^+]} + 1} \quad (5)$$

WT NicC Activity with 4-HBA. Reaction mixtures containing NADH (1 mM), wild-type NicC (320 nM), and varying concentrations of 4-HBA (0.125−5.00 mM) in potassium phosphate buffer (pH 7.5; 100 mM) were incubated at 25 °C for 150 min. Aliquots of the reactions were quenched at specific time intervals over 30 min, and the reaction products were separated with baseline resolution by reverse phase chromatography, as described below. GraFit version 5 was utilized to fit the rate data using nonlinear regression to the Michaelis−Menten equation to determine the apparent steady-state rate constants.

HPLC Sample Preparation. All reactions were quenched with a 1:1 ratio of reaction aliquot (250 μL) and 2 M guanidine hydrochloride (250 μL), and then mixtures filtered by centrifugation (14000*g* for 30 min) to remove the protein using Amicon Ultra centrifugal filters (molecular weight cutoff of 3000, 0.5 mL). The flow-through of each sample containing the small molecules was diluted with water before HPLC analysis.

HPLC Analysis. All NicC reaction mixtures were analyzed using a Shimadzu PSD-M20A 120 V UHPLC instrument equipped with an autosampler, a column oven, and a photodiode array detector. A C18 column (Phenomenex Kinetix 5 μM EVO C18; 150 mm × 4.6 mm) maintained at 30 °C was utilized to separate the reactants and products. The mobile phase incorporated ammonium acetate buffer (pH 7.5, 20 mM) (A) and methanol (B) with the flow rate held constant at 1.0 mL/min. The column was pre-equilibrated in 1% B for 20 min. The following linear gradient was utilized: 1 to 5% B from 0 to 15 min, 5 to 90% B from 15 to 17 min, 90% B from 17 to 19 min, and 90 to 1% B from 19 to 21 min. Equilibration was continued at 1% B for an additional 4 min. Baseline resolution for each molecule was achieved, and the absorbance area of each molecule at its maximum absorbance wavelength (Table S2) was converted to concentration by comparison to a linear plot

DOI: 10.1021/acs.biochem.8b00969
Biochemistry 2019, 58, 1751−1763

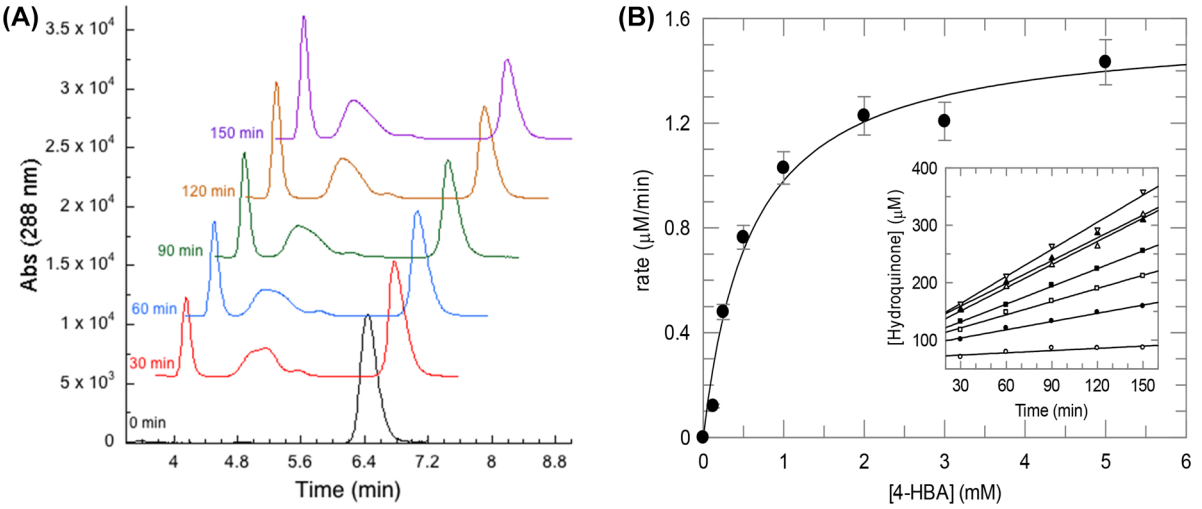

Figure 5. NicC-catalyzed decarboxylative hydroxylation of 4-hydroxybenzoate. (A) HPLC chromatograms showing the formation of the products (hydroquinone t_R = 4.0 min; NAD^+ t_R ~ 4.7 min) and disappearance of NADH (t_R ~ 6.4 min) with time. (B) Michaelis−Menten plot showing the rate of reaction based on the initial rates of hydroquinone formation with time (inset) as a function of increasing 4-hydroxybenzoate concentration. Results of nonlinear regression analysis are listed in Table 1.

Table 1. Comparison of the Reactions Catalyzed by Wild-Type NicC with 6-Hydroxynicotinate (6-HNA) and Substrate Analogues 4-Hydroxybenzoate (4-HBA) and 5-Chloro-6-hydroxynicotinate (5-Cl-6-HNA)[a]

substrate	pK_a (phenol)[b]	k_{cat} (s^{-1})	K_M^S (μM)[d]	k_{cat}/K_M^S (M^{-1} s^{-1})	product coupling ratio[e]	K_d^S (μM)[f]	$^{13}V/K$
6-HNA	11.14 ± 0.07	5.1 ± 0.1	118 ± 12	(4.2 ± 0.8) × 10^4	1	58 ± 12	0.9989 ± 0.0002
4-HBA	9.44 ± 0.02	0.074 ± 0.005[c]	600 ± 100[c]	(1.2 ± 0.3) × 10^{2c}	0.52	355 ± 66	0.9942 ± 0.0004
5-Cl-6-HNA	9.87 ± 0.04	2.18 ± 0.05	3.9 ± 0.5	(5.6 ± 0.7) × 10^5	1	7 ± 2	0.9999 ± 0.0004

[a]The concentration of O_2 was not varied in these assays. All measurements were taken in 50 mM sodium phosphate buffer (pH 7.5) at 25 °C. [b]Ionization of the 6-OH moiety of the substrate measured by following the change in the molecule's absorbance in pH-buffered solutions (Figure S4). [c]Measured by following the initial rate of 2,5-DHP formation by HPLC (Figure 5). [d]With respect to the organic substrate: 6-HNA, 4-HBA, or 5-Cl-6-HNA. [e]The product coupling ratio is defined as the ratio of the initial rates of formation, measured by HPLC, of the hydroxylated product, 2,5-DHP, to that of NAD^+. [f]Equilibrium dissociation constant measured by following the increase in $NicC_{FAD}$ absorbance at 450 nm with addition of 6-HNA (Figure 7), 4-HBA, or 5-Cl-6-HNA (Figure S9).

generated with a dilution series of authentic standards for each molecule (Figure S2).

Dissociation Constants of NicC Substrate Complexes. Titrations of NicC (22−30 μM) with 6-HNA, 4-HBA, or 5-Cl-6-HNA were conducted in 50 mM sodium phosphate buffer (pH 7.5) at 25 °C by following the change in enzyme-bound flavin absorbance at 450 nm using a Shimadzu 1800 dual-beam spectrophotometer. Spectra were determined by subtracting the absorbance changes accompanying NicC in the reference cell titrated with reaction buffer from the absorbance changes in NicC titrated with an equivalent volume of substrate in the sample cell. ΔA_{450} was plotted as a function of total substrate concentration, and the K_d value determined using nonlinear regression analysis to the quadratic binding equation (eq 6) using KaleidaGraph (version 4.1.3):

$$\Delta A = \Delta A_{max}\left\{\left[[NicC]_T + [S]_T + K_d - \sqrt{([NicC]_T + [S]_T + K_d)^2 - 4[NicC]_T[S]_T}\right] / \left(2[NicC]_T\right)\right\} \quad (6)$$

Pyridinol Substrate pK_a Determination. pK_as of the pyridinol or phenol substrates (6-HNA, 5-Cl-6-HNA, and 4-HBA) were measured by changes in ultraviolet (UV) absorbance at 25 °C. Cuvettes containing 1.0 mL of buffer [50 mM MES, HEPES, TAPS, or CAPS titrated to a specific pH (6.1−11.38) with NaOH] or an aqueous NaOH solution (pH >11.38) were blanked. The spectrum was obtained after addition (4 μL) of freshly prepared substrate (final concentration of 100 μM for 6-HNA and 5-Cl-6-HNA or 75 μM for 4-HBA). The pH of the sample was reconfirmed after each absorbance reading. The ΔA [282 nm (4-HBA), 315 nm (6-HNA), or 325 nm (5-Cl-6-HNA)] was plotted as a function of pH and fit to a single-pK_a model (eq 7) with GraFit version 5:

$$y = a + \frac{(b - a) \times 10^{pH-pK_a}}{10^{pH-pK_a} + 1} \quad (7)$$

RESULTS

NicC Activity with Alternative Substrates: 4-HBA and 5-Cl-6-HNA. Wild-type NicC was observed to catalyze the decarboxylative hydroxylation of 4-HBA to hydroquinone (HDQ) (Figure 5). The reaction products were confirmed by their identical chromatographic retention times and UV spectra compared to those of authentic standards. Analyses of the concentrations of the products (NAD^+ and HDQ) by HPLC indicated that the half-reactions of NADH oxidation and decarboxylative hydroxylation of 4-HBA were not coupled ([2,5-DHP]/[NAD^+] product coupling ratio of 0.52 ± 0.08). Thus, the kinetics of the reaction were determined by following the concentration of HDQ formed with time by HPLC. Initial rates of reaction were determined for the formation of the HDQ

DOI: 10.1021/acs.biochem.8b00969
Biochemistry 2019, 58, 1751−1763

Table 2. Comparison of the Apparent Steady-State Kinetic Constants Derived from NADH Oxidation Rates of NicC Active Site Variants[a]

NicC	k_{cat} (s^{-1})	K_M^{6HNA} (μM)	K_M^{NADH} (μM)	k_{cat}/K_M^{6HNA} (M^{-1} s^{-1})	product coupling ratio[b]
WT	5.0 ± 0.1	118 ± 12	8.1 ± 1.6	(4.2 ± 0.8) × 10^4	1.00
C202A	0.26 ± 0.02	200 ± 37	6.3 ± 2.3	(1.3 ± 0.3) × 10^3	0.91
H211A	5.9 ± 0.2	193 ± 39	25 ± 6	(3.1 ± 0.8) × 10^4	0.36
H302A	0.90 ± 0.02	20 ± 7	19 ± 2.5	(4.5 ± 1.6) × 10^4	0.38
Y225F	5.24 ± 0.03	51 ± 8	2.8 ± 1.4	(1.0 ± 0.2) × 10^5	0.52
Y215F	12 ± 9	1600 ± 1500	310 ± 300	(7.5 ± 9.0) × 10^3	0.0048
H47E[c]	–	–	–	–	0.074

[a]Experiments performed in 50 mM sodium phosphate buffer (pH 7.5) and 25 °C without varying the concentration of substrate oxygen (Figure S6). [b]The product coupling ratio is defined as the ratio of the initial rates of formation, measured by HPLC, of 2,5-DHP to that of NAD^+ (Figure S8). Measured with initial concentrations of 1 mM 6-HNA and 100 μM NADH. [c]NicC variants H47A and H47F were unable to bind FAD. H47E bound FAD, but its activity was too low to measure by this continuous spectrophotometric assay.

product (Figure 5, inset) as a function of the initial 4-HBA concentration at a saturating NADH concentration (200 μM). The resulting data were fit to the Michaelis–Menten equation (Figure 5) to determine the apparent steady-state rate constants (Table 1). Comparison of the resulting apparent rate constants shows that 4-HBA is a viable substrate for NicC with a catalytic efficiency (k_{cat}/K_M^{4HBA} = 1.2 × 10^2 M^{-1} s^{-1}) that is 0.29% of that of NicC with its natural substrate, 6-HNA.

Wild-type NicC was observed by HPLC to also catalyze the decarboxylative hydroxylation of 5-chloro-6-hydroxynicotinate to 3-chloro-2,5-dihydroxypyridine with stoichiometric (coupled) oxidation of NADH to NAD^+. Initial rates of reaction were measured spectrophotometrically at a saturating NADH concentration and fit to the Michaelis–Menten equation (Figure S3) to determine the apparent steady-state rate constants (Table 1). Comparison of the k_{cat}/K_M values shows that 5-Cl-6-HNA is transformed 13-fold more efficiently by NicC than is 6-HNA.

Because ionization of the phenolic group of the aromatic substrate has been shown to be important in modulating the conformation of bound flavin for reduction by NADH[14] as well as the electrophilic aromatic hydroxylation of Group A monooxygenases,[18] the pK_a of the pyridinol moiety of 6-HNA, 4-HBA, and 5-Cl-6-HNA was determined spectrophotometrically (Figure S4 and results reported in Table 1). The pK_a measured for 4-HBA (9.44) is in good agreement with the value (9.3)[19] reported earlier for this molecule. Because of the linked keto–enol tautomerization equilibrium, the ioniziation of the 6-OH moiety of 6-HNA is observed to be higher (pK_a = 11.14) in comparison to that of the phenol on benzene derivatives.[18] The substitution of Cl at C5 in 5-Cl-6-HNA causes the pK_a to drop 1.3 pH units from that observed in 6-HNA to 9.87, consistent with earlier observations of the effect (ΔpK_a = −1.6) of a similar Cl substitution (forming 3-Cl-4-hydroxybenzoate) on the pK_a of 4-hydroxybenzoate.[18] These pyridinol pK_as are higher than the pH optimum observed for either steady-state NADH oxidation activity[16] or substrate hydroxylation, suggesting that the pK_a of the substrate is decreased when bound at the active site and that a general base would be important in catalyzing the pyridinol's ionization in the typical hydroxylation mechanism.

^{13}C Kinetic Isotope Effects. The kinetic isotope effect (KIE) on C–C bond cleavage was measured using the internal competition method by determining the $^{12}C/^{13}C$ ratio in isolated product CO_2 by isotope ratio mass spectrometry (IRMS). This method measures the change in the naturally abundant isotopic ratio at varying extents of reaction completion (~30–60%). The observed KIEs for wild-type NicC with three substrates are listed in Table 1 and show good correlation with catalytic efficiency. For the reaction of wild-type NicC with its natural substrate, 6-HNA, the KIE is measurably inverse (0.11%). The KIE becomes more inverse (0.58%) for the reaction of wild-type NicC with the slower substrate, 4-HBA. In contrast, the isotope effect is negligible for the more efficient substrate, 5-Cl-6-HNA.

Mass Spectrometry of NicC with 6-HNA. As hypothesized in one of the mechanistic proposals (blue, Figure 3), 6-HNA may be bound covalently via a Michael addition using the thiolate side chain of Cys202 prior to hydroxylation. ESI-MS was utilized to determine whether the $NicC_{6\text{-}HNA}$ complex was a covalent (ES) complex. All of the ESI-MS spectra were deconvoluted for average molecular weight determination. The deconvoluted spectrum obtained after the analysis of the NicC enzyme showed an average mass of 46576.0 Da (Figure S5), which is consistent with the theoretical molecular weight of a NicC monomer (46468 Da) with six ammonium, $6NH_4^+$ (108 Da), adducts. Given the fact that the enzyme was desalted into ammonium acetate buffer prior to analysis by mass spectrometry, this difference in mass appears to be reasonable. The same ESI-MS analysis of the NicC enzyme preincubated with 6-HNA, or with both 6-HNA and NAD^+, also showed an average mass of 46576.0 Da (Figure S5). A m/z ion of 46713 Da (mass increase of 137 Da) would have been expected if 6-HNA was covalently bound. NAD^+ was added to determine whether the presence of the nicotinamide dinucleotide might stabilize the $NicC_{6\text{-}HNA}$ complex. Addition of NADH would have created a reactive complex that would initiate rapid 6-HNA turnover to 2,5-DHP and prevent the $NicC_{6\text{-}HNA}$ from accumulating. The results of the mass analysis show that NAD^+ had no effect on the observed mass of NicC. These results are consistent with the view that a covalent intermediate is not part of the mechanism or is highly unstable and cannot be preserved upon ESI.

Kinetic Analysis of NicC Active Site Variants. To identify the key catalytic residues in the active site of NicC, the putative active site amino acids, based on the unliganded NicC structure (PDB entry 5EOW), were altered by site-directed mutagenesis and the recombinant enzymes purified successfully by immobilized metal affinity chromatography. The choice of residues to substitute was based on their proximity to the 6-HNA substrate-docked model of the crystal structure of NicC.[16] With the exception of H47A and H47F, each of the purified NicC variants was observed to bind FAD, based on the characteristic absorbance at 450 nm. The steady-state kinetic constants of each NicC variant (H211A, H302A, Y215F, Y225F, and C202A) were measured using a continuous spectrophoto-

DOI: 10.1021/acs.biochem.8b00969
Biochemistry 2019, 58, 1751–1763

metric assay (Michaelis–Menten analysis provided in Figure S6) and are listed in Table 2. Because of the observed very low level of activity of the H47E variant, its apparent catalytic turnover was estimated by the HPLC assay with varying 6-HNA (2.0–20 mM) and NADH (1.0 mM) concentrations (Figure S7B).

The observed effect of changing putative active site residues was highly variable using the spectrophotometric assay that measures the rate of NADH oxidation; some variants were observed to have decreased rates of catalytic turnover (e.g., the C202A and H47E variants retained only 5% and 0.28%, respectively, of k_{cat} compared to that of the wild type), whereas other variants showed little effect or perhaps a slightly increased rate of catalytic turnover compared with that of the wild type. Similarly, the variants' effect on the K_M value of each substrate was also observed to be variable, with the largest effect observed for the Y215F variant in which the K_M for 6-HNA was estimated to increase ~10-fold. Given the large increase in K_M observed for Y215F as well as the larger errors associated with its global fit to the ternary complex rate equation, it is likely that the k_{cat} value estimated for Y215F is overestimated.

To better discern whether the active site variants affected the rate of turnover of 6-HNA, a discontinuous HPLC-based assay was developed to separate and quantify the extent of formation of both products, NAD^+ and 2,5-DHP. The extents of formation of NAD^+ and 2,5-DHP were determined from integration of the corresponding peaks on the HPLC chromatograms. The ratio of the initial rates of 2,5-DHP formation to NAD^+ formation (Figure 6 and Figure S8) was used to establish a product coupling factor (Table 2). For wild-type NicC, the concentrations of 2,5-DHP and NAD^+ produced were observed to be equivalent over 20 min (i.e., the formation of 2,5-DHP was shown to be strictly coupled to the formation of NAD^+) (Figure 6); therefore, the product coupling factor was measured as 1.00. Likewise, the stoichiometry of the products formed with the C202A variant was ~1:1 (Figure 6C), indicating that this NicC variant retained efficient substrate hydroxylation activity. Substitution of other active site residues, Y225F, H211A, and H302A, showed moderate uncoupling of their rates of NAD^+ and 2,5-DHP product formation, suggesting that these variants had lost some efficiency in hydroxylating the substrate. In contrast, the Y215F and H47E variants showed (Figure 6D,E) significant consequences in their hydroxylating activity, with NADH oxidization proceeding much more rapidly than 6-HNA is decarboxylated and hydroxylated.

Because of the observed effects of decoupling, the steady-state rate constant for producing the hydroxylated product, 2,5-DHP, was remeasured using the HPLC assay for each variant under the exact same conditions that were used for wild-type NicC. This experimental design permitted a direct measure and comparison of the kinetic consequences of each substitution to catalysis. The initial rates of 2,5-DHP formation in this assay fit to linear regression analysis (Figure S7), and the relative multiturnover rate constant (k_{OH}) for each variant is reported in Table 3. The observed k_{OH} values for all of the enzymes, except the H47E variant, remained within 10% of the original value when remeasured using this assay with 2.5 times more 6-HNA (5.0 mM), suggesting that the observed k_{OH} is a first-order rate constant. For the H47E variant, the observed k_{OH} value increased linearly with an increasing 6-HNA concentration through 20 mM (Figure S7B), suggesting that this variant's affinity for 6-HNA was dramatically reduced (consistent with K_d measurements described below). The apparent second-order

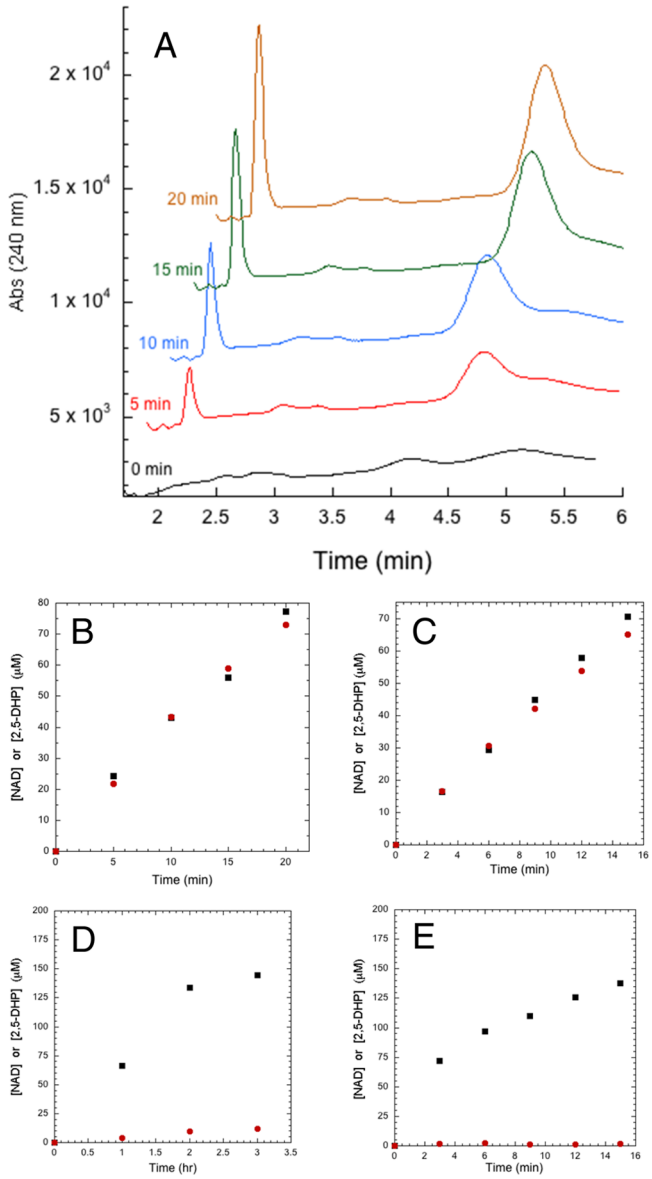

Figure 6. Analysis of the stoichiometry (coupling) of the products of NicC-catalyzed reactions. (A) HPLC chromatograms showing the formation and separation of 2,5-dihydroxypyridine (t_R = 2.0 min) and NAD^+ (t_R ~ 4.7 min) with time with wild-type NicC. Plots B–E show the resulting analyses of the concentrations of NAD^+ (black squares) and 2,5-dihydroxypyridine (red circles) as a function of time for (B) wild-type NicC, (C) C202A, (D) H47E, and (E) Y215F. Plots B and C illustrate product coupling (1:1 stoichiometric formation of NAD^+ and 2,5-DHP), whereas plots D and E illustrate uncoupling of product formation (NAD^+ formation without significant 2,5-DHP formation). Effects of the other NicC variants (Y225F, H302A, and H211A) on the relative rates of product formation are shown in Figure S8, with all product coupling ratios reported in Table 2.

rate constant (2.3×10^{-1} M^{-1} s^{-1}) for the H47E variant is 10^5-fold lower than the k_{cat}/K_M value of wild-type NicC. The relative k_{OH} values show that the C202A, H211A, and Y225F variants retain the ability to catalyze 6-HNA hydroxylation and further implicate H302, Y215, and H47 as being critical determinants of the hydroxylation steps in catalysis. Of these three enzymes, the Y215F variant has an ability similar to that of the wild type to oxidize NADH (relative k_{NAD} reduced 50% in the Y215F variant), but its ability to transfer the hydroxyl group onto the

DOI: 10.1021/acs.biochem.8b00969
Biochemistry 2019, 58, 1751–1763

Table 3. Comparison of the Initial Steady-State Rates of Product (2,5-DHP and NAD^+) Formation Measured by HPLC and Equilibrium Dissociation Constants for the $NicC^{6HNA}_{FAD}$ Complex[a]

NicC	relative k_{OH} (s^{-1})[b]	relative k_{NAD} (s^{-1})[b]	K_d^{6HNA} (μM)[c]
WT	1.00	1.00	58 ± 12
C202A	0.85	0.76	97 ± 11
H211A	0.91	0.96	1500 ± 200
H302A	0.09	0.16	3700 ± 400
Y225F	0.82	0.85	75 ± 34
Y215F	0.00047	0.54	14000 ± 5000
H47E[d]	0.00022	0.0011	high, >20000

[a]Experiments performed in 50 mM sodium phosphate buffer (pH 7.5) at 25 °C without varying the concentration of substrate oxygen. [b]Relative rate constant for the formation of 2,5-DHP (k_{OH}) or NAD^+ (k_{NAD}) measured from linear initial rates using 25 nM NicC, 1 mM NADH, and 2 mM 6-HNA (Figure S7A) over a 20 min time interval. The initial rate was divided by $[E]_T$ to determine the rate constant (k_{OH} or k_{NAD}). [c]Dissociation constants measured spectrophotometrically following the increase in $NicC_{FAD}$ absorbance at 450 nm with 6-HNA (Figure 7 and Figure S9). K_d values reported are the average and standard deviation of two or three independent titrations. [d]H47E variant (500 nM) with 2 mM 6-HNA and 1 mM NADH measured over a 25 h time interval. The observed initial rate showed a linear dependence on the concentration of 6-HNA through 20 mM, with a second-order rate constant of (2.3 ± 0.1) × 10^{-1} M^{-1} s^{-1} (Figure S7B).

organic substrate was greatly diminished (relative k_{OH} is 0.05% of that of the wild type). This result is consistent with the observed small product coupling factor observed for Y215F. Likewise, the H47E variant showed a drastically reduced observed k_{OH} compared to that for the wild-type enzyme at 2 mM 6-HNA (relative k_{OH} of 0.02%), but unlike the Y215F variant, H47E also showed a pronounced effect on the enzyme's ability to oxidize NADH (relative k_{NAD} is 0.1% of the wild-type value).

Effects of NicC Active Site Variants on K_d^{6HNA}. Equilibrium dissociation constants for the E^{6HNA}_{FAD} complex were measured spectrophotometrically following the changes in absorbance of the enzyme-bound flavin at 450 nm by titration with 6-HNA (Figure 7 and Figure S8). Nonlinear regression analysis of the data to the quadratic binding equation provided estimates of the K_d^{6HNA} value with reasonable error in all cases except for the Y215F and H47E variants. Values of K_d^{6HNA} (Table 3) are reported as averages and standard deviations of two or three individual titrations. From this analysis, it is apparent that Y215 and H47 are critical determinants in NicC's affinity for 6-HNA. These results are consistent with the observed increase in K_M^{6HNA} measured by the continuous NADH oxidation assay for these variants. NicC variants C202A and Y225F show marginal loss of affinity for 6-HNA compared to that of the wild-type enzyme, whereas the effects of the H211A and H302A variants are slightly more pronounced. Given the observation that the k_{OH} value remained constant with an increase in concentration of 6-HNA from 2.0 to 5.0 mM for wild-type NicC and all of the NicC variants except H47E, these data also suggest that NicC's affinity for 6-HNA may increase when NADH is saturating.

DISCUSSION

Oxidation is a fundamental reaction that organisms use to catabolize nutrients. In the bacterial degradation of NHACs, the oxidation and hydroxylation of the aromatic ring promote its opening and facilitate its conversion to common metabolites to provide carbon and energy for the bacteria. The mechanisms and specificity of Group A flavin monooxygenases, a class of enzyme that adds a single oxygen atom from O_2 to an organic substrate, are of particular interest as these enzymes have applicability in both biosynthesis and biodegradation, and highlight how catalysts evolved to serve in novel synthetic pathways.[20] Given that there are only three known Group A FMOs that catalyze C−C bond cleavage in addition to hydroxylation of a pyridine substrate [NicC, HpaM,[21] and HspB[22] (see Figure S1)], it is of interest to discern whether these enzymes follow mechanistic principles similar to those of the Group A FMOs that catalyze a similar reaction with homocyclic phenols. Of these three enzymes (NicC, HpaM, and HspB), only NicC has a reported protein structure[16] and only the kinetic mechanism of wild-type HspB[22] has been investigated. Thus, the structural determinants of substrate specificity and catalysis involving this subset of Group A FMOs are currently unknown. Initial structural and kinetic investigations of NicC[16] supported the proposal of two potential mechanisms for the oxidative half-reaction [starting with the C(4a)-hydroperoxy flavin intermediate] (Figure 3). Results of this work provide functional evidence in support of an electrophilic aromatic substitution mechanism without the involvement of thiolate addition and identify the catalytic roles of several active site residues.

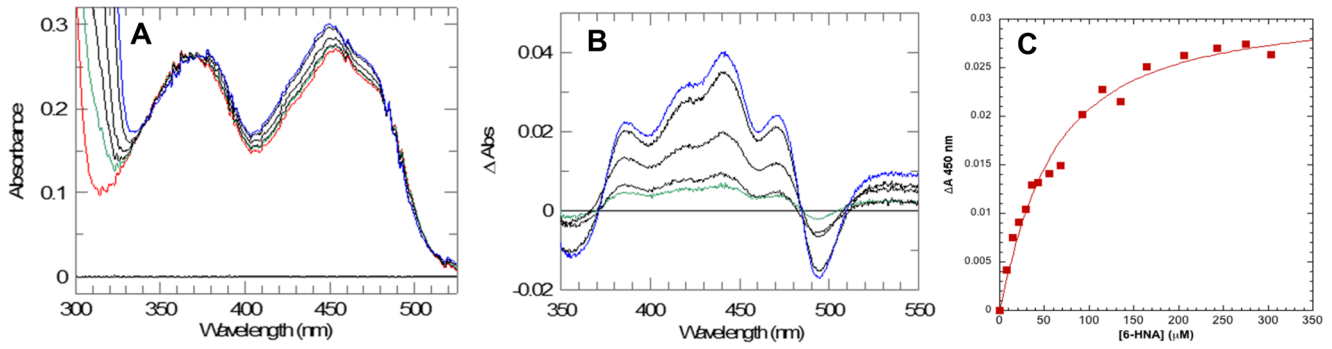

Figure 7. Determination of the K_d^{6HNA} of the $NicC^{6HNA}_{FAD}$ complex by following the increase in absorbance (450 nm) of bound FAD upon titration of NicC with 6-HNA in sodium phosphate buffer (50 mM, pH 7.5) at 25 °C. (A) Absorbance spectra of the NicC-bound flavin (22 μM). (B) Difference spectra showing the changes in absorbance of the enzyme-bound flavin due to binding of 6-HNA [from 30 (green) to 1000 (blue) μM]. (C) Representative titration of wild-type NicC with 6-HNA showing results of nonlinear regression analysis (eq 6), estimating a K_d^{6HNA} of 41 ± 6 μM. Results of titrations of wild-type NicC with alternative substrates and of NicC variants with 6-HNA are shown in Figure S9.

DOI: 10.1021/acs.biochem.8b00969
Biochemistry 2019, 58, 1751−1763

On the basis of previous observations that thiol-reacting compounds completely inhibit NicC activity[23] and that NicC catalytic turnover is partially and reversibly reduced by MMTS,[16] a mechanism initially involving the covalent addition of Cys202 to 6-HNA was proposed (Figure 3). Numerous spectroscopic, theoretical, and structural studies of 2-pyridone and its 6-substituted derivatives indicate that the 6-oxo tautomer is preferred in solution when the pyridine ring lacks substituents at C2 or contains electron-donating substituents at this position.[24] Michael addition by Cys202 would generate a phenolic oxyanion intermediate that could further enable hydroxylation at C3 using the C(4a)-hydroperoxy flavin as the oxygen source. Subsequent decarboxylation would promote thiolate dissociation, enable rearomatization, and produce 2,5-DHP.

To determine the importance of the 6-oxo tautomer in this reaction mechanism, 4-hydroxybenzoate (4-HBA), a homocyclic analogue of 6-HNA that is unable to form the keto tautomer spontaneously in a neutral solution, was examined as a potential NicC substrate. Analysis of the hydroquinone product with time by HPLC shows that 4-HBA is decarboxylated and hydroxylated to hydroquinone with a k_{cat}/K_M of 1.2×10^2 M^{-1} s^{-1} (Figure 5). Although the catalytic efficiency of NicC with 4-HBA is ~200-fold lower than that of NicC with 6-HNA, 4-HBA is observed to be a viable substrate. Because 4-HBA cannot proceed through the mechanism with a keto tautomer at C6, this result negates that mechanistic requirement. To discern whether the mechanisms of NicC with 4-HBA and 6-HNA are similar, the primary ^{13}C kinetic isotope effect ($^{13}V/K$), which reports on the structure of the transition state for C−C bond cleavage for irreversible decarboxylation, was measured for each substrate. Intriguingly, the $^{13}V/K$ was observed to be measurably inverse (<1) for both substrates, with the effect being more pronounced for the slower substrate, 4-HBA (0.58%), than for the natural substrate, 6-HNA (0.11%). These inverse effects indicate that the two substrates undergo similar mechanisms of decarboxylation. In accord with this view, 5-chloro-6-hydroxynicotinate, observed to be a more efficient (~10-fold) substrate with NicC than 6-HNA, showed a negligible isotope effect (~1.000) (Table 1). Unlike 4-HBA, which caused an ~50% uncoupling of the NADH oxidation rate from the hydroxylation rate, the decarboxylative hydroxylation of 5-Cl-6-HNA, like that with 6-HNA, is observed to be coupled with NADH oxidation. These observed inverse and negligible kinetic isotope effects indicate that secondary isotope effects dominate the primary kinetic isotope effect for this C−C bond cleavage mechanism. That result can be rationalized by an intermediate whose formation is favored by ^{13}C and reacts with a high commitment for decarboxylation. Addition of the -OH group would change the hybridization at C3 from sp^2 to sp^3 (an equilibrium favored by ^{13}C). Thus, if decarboxylation then proceeds from this tetrahedral intermediate more quickly than it returns to the substrate, the inverse isotope effects observed for these reactions appear to be explicable. The 10-fold rate enhancement observed for Cl substitution at C5 of the pyridine ring in 5-Cl-6HNA, theoretically increasing slightly the electron density at the ortho/para (C4, C6/C2) positions and contributing a strong electron-withdrawing inductive effect in the pyridine ring, is inconsistent with covalent addition of a thiolate at C2 but would be consistent with the electrophilic aromatic substitution mechanism involving general base catalysis.

In addition, the enhanced activity of the 5-Cl-6-HNA over 6-HNA follows the observed trend in the ionization equilibrium of the pyridinol moiety (Table 1). The commonly accepted mechanism of *p*-hydroxylases involves ionization of the phenol to increase electron density in the benzene ring to promote the electrophilic aromatic attack on the terminal electrophilic oxygen of the C(4a)-hydroperoxy flavin intermediate.[18,25] The observation that 5-Cl-6-HNA is a better substrate than 6-HNA, in which 5-Cl-6-HNA has a lower pK_a of the 6-OH group and a greater binding affinity than 6-HNA, is in agreement with a more comprehensive trend observed earlier for 4-hydroxybenzoate 1-hydroxylase (UniProtKB entry G8B709) with similar substrate analogues[18] and is consistent with phenol deprotonation being important in substrate binding and hydroxylation.[a] Although the $^{13}V/K$ cannot distinguish between the two mechanisms proposed here (Figure 3), as each involves a tetrahedral intermediate prior to decarboxylation, the observations of a negligible $^{13}V/K$ for decarboxylation with 5-Cl-6-HNA with a lower phenol pK_a and the very high pK_a of 6-HNA with an inverse $^{13}V/K$ for decarboxylation suggest that a step in substrate hydroxylation (involving deprotonation at 6-OH and subsequent addition of -OH at C3 to form the tetrahedral intermediate) may constitute the rate-limiting step leading to substrate decarboxylation in NicC. In agreement with that view, analysis of the rate constants by stopped-flow spectrophotometry of the kinetic mechanism of HspB[22] showed that the overall observed first-order rate constant of C(4a)-hydroperoxy flavin oxidation in forming the hydroxylated product appeared to be the decay of that intermediate (i.e., hydroxylation of the substrate).

Additional functional studies are in accord with the results from kinetic analysis of substrate analogues discussed above and help to discern the mechanism of NicC. Covalently bound intermediates are not observed by mass spectrometry analyses of NicC with 6-HNA, either with or without NAD^+ (Figure S5). Likewise, the relative hydroxylation rate constant (k_{OH}) of the C202A variant of NicC is 85% of that for wild-type NicC, showing that the thiolate side chain is unnecessary because its removal does not result in a significant loss of activity one would otherwise expect from losing a catalytic nucleophile. Given this observation and the current crystal structure of NicC showing that Cys202 is distant (~10 Å) from the putative 6-HNA binding site,[16] the direct involvement of the thiolate in the decarboxylative hydroxylation reaction is unlikely. In total, results of these studies provide strong evidence that negates the requirement of the 6-oxo tautomer, or alternative mechanisms requiring the ring nitrogen, and greatly reduces the likelihood that the mechanism of NicC involves covalent intermediates. Thus, the NicC-catalyzed reaction likely follows an electrophilic aromatic substitution mechanism that is commonly accepted for FMOs with phenolic substrates.

The current, high-resolution X-ray structure of NicC[16] is of the flavin enzyme without 6-HNA bound. The putative site for 6-HNA binding was postulated on the basis of an energy-minimized docking model using Glide[26] that placed 6-HNA within 5.3 Å of the C(4a) atom of the flavin isoalloxazine ring. This model predicted that a number of conserved histidine and tyrosine (H47, H211, H302, Y215, and Y225) residues lined the 6-HNA binding site. Examination of the NicC active site for potential catalytically important residues based on sequence homology to other flavin monooxygenases[16] indicates that the putative active site of NicC most resembles that of 3-hydroxybenzoate 6-hydroxylase (3HB6H, UniProtKB entry Q0SFK6). The structure of 3HB6H was determined in the presence of its substrate, 3-hydroxybenzoic acid.[27] Both NicC

DOI: 10.1021/acs.biochem.8b00969
Biochemistry 2019, 58, 1751−1763

and 3HB6H contain tyrosine residues and histidine residues that are proposed to play roles in catalysis and substrate binding. Specifically, Tyr215 and His211 in NicC correspond to the catalytically important Tyr217 and His213, respectively, in 3HB6H.[28] In addition, 3HB6H also has a glutamine (Gln49) that is proposed to be involved in catalysis, while NicC does not contain a similar residue at that position in its active site. Furthermore, His211 in NicC also is in a position similar to that of the active site base (His202) in 2,6-dihydroxypyridine 3-hydroxylase (UniProtKB entry Q93NG3).[29]

Although salicylate hydroxylase (SAH, UniProtKB entry P23262) also catalyzes a mechanism that could involve a decarboxylative hydroxylation on the same carbon,[30] NicC is limited in its active site structural similarity to SAH, in which arginine, glutamine, and serine residues are involved in catalysis (see Figure 7A in ref 16). Likewise, NicC also has no significant sequence or structural homology to 3-hydroxybenzoate hydroxylase (MHBH, UniProtKB entry Q6SSJ6) (<10% query coverage), which catalyzes the *para* hydroxylation of 3-hydroxybenzoate to 3,4-dihydroxybenzoate. However, on the basis of the liganded structure of MHBH,[31] this enzyme is also proposed to contain catalytically important histidine and tyrosine residues (His135 and Tyr271) as well as aspartate and lysine residues.

On the basis of the proposed structural model and structural alignments with other Group A FMOs, His211 was initially predicted to be the general base catalyst.[16] This potential assignment also agreed with the pH dependence of NicC activity[16] that indicated the probable importance of a general base with an effective pK_a of 7.2, consistent with a possible role for histidine in catalysis. To test this hypothesis and further establish the active site determinants of NicC catalysis, a series of active site variants were created and their effects on the apparent steady-state kinetic parameters for both NADH oxidation and 6-HNA decarboxylative hydroxylation were determined (Tables 2 and 3).

The activities of the NicC active site variants determined by the NADH oxidation assay (Table 2) suggest that Cys202, Tyr215, and His47, are important residues in catalysis. Because of the involvement of multiple kinetic steps in the mechanism after NADH reduces FAD and, moreover, because the resulting C(4a) hydroperoxy flavin intermediate has two kinetically viable pathways for turnover, only one involving hydroxylation and decarboxylation of the organic substrate (6-HNA), further kinetic experiments were designed to determine whether any of the variants affected the rate of 2,5-DHP formation.

The ratio of the initial rates of 2,5-DHP formation to NAD^+ formation was measured to establish a product coupling factor (Table 2). This factor ranged from 1.0 (indicating stoichiometric formation of NAD^+ and 2,5-DHP) for wild-type NicC to 0.074 (indicating faster NADH oxidation than 2,5-DHP formation) for the H47E NicC. The results indicate that Tyr215 and His47 are clearly critical for catalysis and are likely involved in the mechanistic steps of 6-HNA hydroxylation. As further evidence of this possibility, the relative steady-state rate constants for the formation of the products (k_{NAD} and k_{OH}) (Table 3) show clearly that the hydroxylating efficiency of the Y215F and H47E variants is significantly compromised. Whereas the Y215F variant was observed to oxidize NADH relatively rapidly (k_{NAD} down only 50% compared to that of the wild type), the H47E variant's ability to oxidize NADH was also significantly compromised (k_{NAD} observed to be 0.1% of that of the wild type). Because 6-HNA binding is observed to enhance the wild-type NicC's steady-state rate of NADH oxidation 30-fold, the observed decrease in k_{NAD} in the H47E variant may be at least partially explained by its lower binding affinity (K_d is >350-fold greater than that of the wild type) for 6-HNA (Table 3). The Y215F variant showed the next greatest loss (ΔK_d of ~200-fold compared to that of the wild type) in 6-HNA binding affinity. In comparison, the H211A variant had a negligible effect on k_{OH} and k_{NAD} (91% and 96%, respectively, of that of the wild type), and only a modest decrease in binding affinity for 6-HNA (ΔK_d of 26-fold compared to that of the wild type). It is clear from these functional analyses that His47, instead of His211, and Tyr215 are critical for substrate binding and hydroxylation. Apart from the observation that Tyr217 in 3HB6H (analogous to Tyr215 in NicC) was also shown to be critical in substrate binding,[28] the closest structural homologues do not predict correctly the catalytically important residues in NicC.

Among the other structural homologues of NicC is *p*-hydroxybenzoate hydroxylase (PHBH, UniProtKB entry P00438) which shares 20% sequence identity with NicC. Structural[32] and kinetic[33,34] studies of PHBH indicate that an H-bonding network, consisting of His72, Tyr385, Tyr201, and water molecules, serves to modulate conformations that change active site access to the flavin as well as the ionization of the phenolic substrate. Precise control of the generation and access to the C(4a) hydroperoxy flavin intermediate is critical to the specificity and efficiency of Group A monooxygenases. Given the structural similarities between PHBH and NicC, and the kinetic consequences to catalysis of the NicC variants reported here, it appears possible that the hydroxylation−decarboxylation mechanism catalyzed by NicC proceeds via a similar electrophilic aromatic substitution involving an H-bonding network. Consistent with this possibility, the rate constant (k_{OH}) for forming the 2,5-DHP product in wild-type NicC fits a double-bell pH profile with pK_as of 7.7 and 10.1 (Figure 8). The pK_a

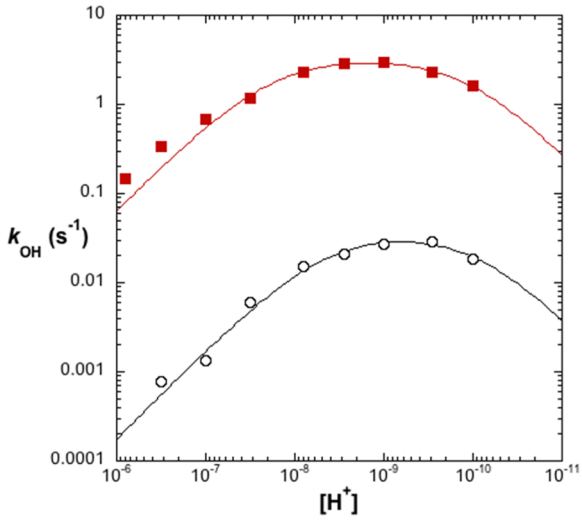

Figure 8. pH dependence of the steady-state rate constant for formation of the hydroxylated product (2,5-DHP) catalyzed by wild-type (red squares) and Y215F (empty circles). k_{OH} values determined from linear regression analysis of the initial rate of 2,5-DHP formation measured by HPLC analysis with six measurements over a 20 min time interval with 6-HNA (2 mM), NADH (1 mM), and either wild-type NicC (25 nM) or Y215F NicC (200 nM) in a mixed buffer system. Rate constants fit to a double-bell curve pH−rate profile with pK_as of 7.71 ± 0.06 and 9.9 ± 0.1 for wild-type NicC and pK_as of 8.3 ± 0.1 and 10.1 ± 0.1 for Y215F NicC.

DOI: 10.1021/acs.biochem.8b00969
Biochemistry 2019, 58, 1751−1763

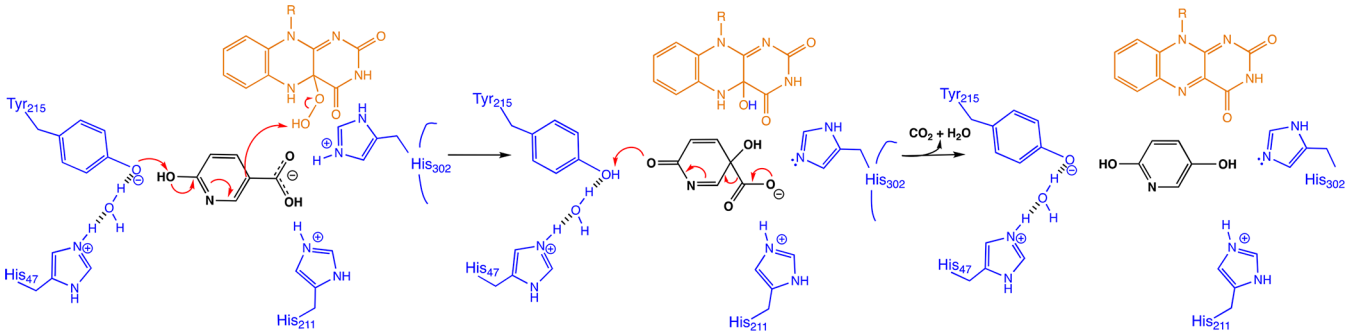

Figure 9. Proposed mechanism of the NicC-catalyzed decarboxylative hydroxylation half-reaction illustrating an H-bonding network, involving Y215 and H47 with an intervening water molecule, that functions as a general base catalyst in the hydroxylation of 6-HNA. H211 and H302 are shown as important contributors to carboxylate binding, with H302 potentially positioned to also serve as the proton donor in the generation of the FADHOH intermediate.

reported for a similar Tyr-His network in the active site of PHBH (7.1−7.2)[33,34] is in satisfactory agreement with the lower pK_a (7.7) reported here. A similar pH profile is observed for the Y215F variant of NicC (Figure 8), with the exception that the lower observed pK_a is increased to 8.3 (ΔpK_a = +0.6 compared to that of the wild type).[b] In light of the kinetic and substrate binding effects of the Y215F variant, the slightly increased observed pK_a suggests that Tyr215 may provide some stabilization of the phenolate ion and that His47 is likely the critical active site base that initiates abstraction of a proton from 6-HNA. Determining whether H47 uses an H-bonding network involving a water molecule and the phenol side chain of Tyr215 (Figure 9), as in the case of PHBH,[33] or directly deprotonates the 6-OH group with Tyr215 serving to stabilize the resulting phenolate intermediate requires additional structural data of a NicC−substrate complex.

The functional data from the variants characterized here suggest that the 6-HNA docked model of the NicC active site predicted previously,[16] with the 6-OH group of 6-HNA oriented within H-bonding distance of His211, is likely incorrect. Instead, the orientation of bound 6-HNA likely needs to be flipped 180° in that original model, positioning the 6-OH within H-bonding distance of Tyr215 rather than His211. Manual placement of the 6-HNA in this orientation within the NicC structure places the C(4a) of the hydroperoxyl flavin intermediate approximately 5.6 Å from the carboxylate of 6-HNA (Figure S10). This distance is consistent with other ligand-bound structures of flavin monooxygenases[35,36] and would enable electrophilic aromatic substitution to be catalyzed by abstraction of the phenolic proton at 6-OH by Tyr215-His47. The role of His211 in the active site of NicC could be to aid in the formation of the NicC−6-HNA complex by H-bonding with the carboxylate of 6-HNA. Loss of that potential interaction in the H211A variant is observed to maintain most of the catalytic activity observed by the wild-type enzyme, indicating that the active site structure appears largely intact in this variant, but slightly decreases the enzyme's affinity for 6-HNA. The importance of the carboxyl group of 6-HNA in binding by NicC was highlighted earlier by the high K_I (3000 μM) of 6-hydroxynicotinaldehyde,[16] compared to the K_M (120 μM) or K_d (60 μM) of 6-HNA. In addition, characterization of the effects of the H302A variant, showing an even stronger effect on the enzyme's affinity for 6-HNA (K_d^{6HNA} increases 64-fold in comparison to that of the wild type) and a significant decrease in the relative hydroxylation and NADH oxidation rate constants (k_{OH} and k_{NAD} being 9% and 16% of that of the wild type, respectively), suggests that His302 is also important in substrate recognition and catalysis. Being present on a structured loop at the active site of NicC, His302 may play a role in coordinating conformational changes that help regulate rates of FAD reduction and oxidation. The next stage of this work is focused on using the active site variants and substrate analogues described here to capture and determine the precise X-ray structure of the NicC−6HNA complex as well as to determine the exact kinetic effects of these variants by transient-state kinetic measurements.

■ ASSOCIATED CONTENT

Supporting Information

The Supporting Information is available free of charge on the ACS Publications website at DOI: 10.1021/acs.biochem.8b00969.

Reactions of all known Group A FMOs that catalyze C−C bond cleavage hydroxylation reactions on aromatic substrates; primers used for site-directed mutagenesis of the NicC gene; HPLC elution times and λ_{max} values for all NicC reactants and products; standard curve for converting HPLC-eluted peak integrals to molar concentration; Michaelis−Menten plots of NicC activity with 5-Cl-6HNA; LC-ESI mass spectra of NicC with and without 6-HNA; Michaelis−Menten plots of NicC activity of the wild type and active site variants; comparison of the initial rates of NAD^+ and 2,5-DHP production by NicC variants to determine the product coupling factors; titrations of wild-type NicC with 6-HNA, 4-HBA, and 5-Cl-6-HNA as well as titration of active site variants of NicC with 6-HNA; and a new structural model for the binding of 6-HNA in the active site of NicC and the effects of the active site variants (PDF)

Accession Codes

B. bronchiseptica RB50 6-hydroxynicotinate 3-monooxygenase (NicC), A0A0H3LKL4; *P. putida* KT2440 6-hydroxynicotinate 3-monooxygenase (NicC), Q88FY2; *Alcaligenes faecalis* 5-hydroxypicolinate 3-monooxygenase (HpaM), A0A223A361; *Rhodococcus jostii* RHA1 3-hydroxybenzoate 6-hydroxlyase (3HB6H), Q0SFK6; *Pseudomonas fluorescens* *p*-hydroxybenzoate hydroxylase (PHBH), P00438; *Paenarthrobacter nicotinovarans* 2,6-dihydroxypyridine 3-monooxygenase, Q93NG3; *P. putida* salicylate hydroxylase (SAH), P23262; *Comamonas testosteroni* 3-hydroxybenzoate hydroxlyase (MHBH), Q6SSJ6; *P. putida* 6-hydroxy-3-succinoylpyridine 3-monooxygenase

DOI: 10.1021/acs.biochem.8b00969
Biochemistry 2019, 58, 1751−1763

(HspB), F8G0M4; *Candida parapsilosis* 4-hydroxybenzoate 1-monooxygenase, G8B709.

AUTHOR INFORMATION

Corresponding Author

*E-mail: msnider@wooster.edu. Phone: 330-263-2391.

ORCID

Chrys Wesdemiotis: 0000-0002-7916-4782

Mark J. Snider: 0000-0003-1054-1276

Funding

Research at The College of Wooster was supported by National Science Foundation (NSF) Grant 1817535 as well as a Henry Luce III Grant for Distinguished Scholarship to M.J.S., Henry J. Copeland Funds for Senior Independent Study to K.D.N., R.G.C., and T.J.G., and Sophomore Research Funding to S.W.P. Research at The State University of New York College at Cortland was partially supported by NSF Grant 1817633. The study of kinetic isotope effects was supported by National Institutes of Health Grant GM01938-38.

Notes

The authors declare no competing financial interest.

ACKNOWLEDGMENTS

The authors gratefully acknowledge the late Professor Mo Cleland (University of Wisconsin) for his support in our measurements of the kinetic isotope effects. Additionally, the authors thank Alvi Sakib and Jack Harrington, former students at The College of Wooster who collected kinetic data on some of the NicC variants, and Professor Zack Matesich (The College of Wooster) for helpful conversations during the preparation of the manuscript. The authors also thank the University of Akron Mass Spectrometric Facility for the mass spectrometry data.

ABBREVIATIONS

6-HNA, 6-hydroxynicotinic acid; 2,5-DHP, 2,5-dihydroxypyridine; 4-HBA, 4-hydroxybenzoic acid; HDQ, hydroquinone; 5-Cl-6HNA, 5-chloro-6-hydroxynicotinic acid;; NA, nicotinic acid; KIE, kinetic isotope effect; IPTG, isopropyl β-D-thiogalactopyranoside; FAD, flavin adenine dinucleotide; PHBH, *p*-hydroxybenzoate hydroxylase; HpaM, 5-hydroxypicolinate 3-monooxygenase; 3HB6H, 3-hydroxybenzoate 6-hydroxylase; MHBH, 3-hydroxybenzoate hydroxlyase; SAH, salicylate hydroxylase; HspB, 6-hydroxy-3-succinoylpyridine 3-monooxygenase; NHACs, N-heterocyclic aromatic compounds; NADH, nicotinamide adenine dinucleotide (reduced form); NAD^+, nicotinamide adenine dinucleotide (oxidized form); ESI-TOF-MS, electrospray ionization time-of-flight mass spectrometry; FMO, flavin monooxygenase; FPLC, fast protein liquid chromatography; HPLC, high-pressure liquid chromatography; IRMS, isotope ratio mass spectrometry.

ADDITIONAL NOTES

[a]Although the absence of the ring nitrogen in 4-HBA causes this analogue to lose some binding affinity and to be hydroxylated and decarboxylated less efficiently than 6-HNA, its chlorinated analogue, 3-chloro-4-hydroxybenzoate (pK_a = 7.7),[18] would be predicted to be a better substrate because of its lower pK_a. Preliminary results are in accord with this prediction, suggesting that the observed catalytic efficiency of NicC with 3-chloro-4-hydroxybenzoate is 5.3×10^5 M^{-1} s^{-1} (5000-fold greater than that measured with 4-HBA).

[b]Although detectable, the activity of the H47E variant was not stable long enough to be analyzed as a function of pH. In addition, H47E could not be saturated with 6-HNA for a pH profile comparable to that of the wild type or Y215F. It is also worth noting that the neutralized variants at His47 (H47A and H47F) lost the ability to bind FAD, and thus, their activity could not be measured, suggesting that the role for H47 in NicC may also involve coordinating active site conformations that are important for modulating flavin chemistry. The observation that the H47E variant, having a negatively charged side chain, retains FAD binding and measurable activity further supports the possible role of H47 in serving as a general base catalyst.

REFERENCES

(1) Focazio, M. J., Kolpin, D. W., Barnes, K. K., Furlong, E. T., Meyer, M. T., Zaugg, S. D., Barber, L. B., and Thurman, M. E. (2008) A national reconnaissance for pharmaceuticals and other organic wastewater contaminants in the United States — II) Untreated drinking water sources. *Sci. Total Environ. 402* (2−3), 201−216.

(2) Barnes, K. K., Kolpin, D. W., Furlong, E. T., Zaugg, S. D., Meyer, M. T., and Barber, L. B. (2008) A national reconnaissance of pharmaceuticals and other organic wastewater contaminants in the United States - I) Groundwater. *Sci. Total Environ. 402* (2−3), 192−200.

(3) Seo, J. S., Keum, Y. S., and Li, Q. X. (2009) Bacterial degradation of aromatic compounds. *Int. J. Environ. Res. Public Health 6* (1), 278−309.

(4) Bleeker, E. A. J., Van Der Geest, H. G., Klamer, H. J. C., De Voogt, P., Wind, E., and Kraak, M. H. S. (1999) Toxic and genotoxic effects of azaarenes: isomers and metabolites. *Polycyclic Aromat. Compd. 13* (3), 191−203.

(5) Fetzner, S. (1998) Bacterial degradation of pyridine, indole, quinoline, and their derivatives under different redox conditions. *Appl. Microbiol. Biotechnol. 49* (3), 237−250.

(6) Kaiser, J. P., Feng, Y., and Bollag, J. M. (1996) Microbial metabolism of pyridine, quinoline, acridine, and their derivatives under aerobic and anaerobic conditions. *Microbiol. Rev. 60* (3), 483−498.

(7) Fetzner, S. (2000) Enzymes Involved in the Aerobic Bacterial Degradation of *N*-Heteroaromatic Compounds: Molybdenum Hydroxylases and Ring-Opening 2,4-Dioxygenases. *Naturwissenschaften 87* (2), 59−69.

(8) Hunt, A. L., Hughes, D. E., and Lowenstein, J. M. (1958) The hydroxylation of nicotinic acid by *Pseudomonas fluorescens*. *Biochem. J. 69* (2), 170−173.

(9) Holcenberg, J. S., and Stadtman, E. R. (1969) Nicotinic acid metabolism III. Purification and properties of a nicotinic acid hydroxylase. *J. Biol. Chem. 244* (5), 1194−1203.

(10) Nagel, M., and Andreesen, J. R. (1990) Purification and characterization of the molybdoenzymes nicotinate dehydrogenase and 6-hydroxynicotinate dehydrogenase from *Bacillus niacini*. *Arch. Microbiol. 154* (6), 605−613.

(11) Behrman, E. J., and Stanier, R. Y. (1957) The bacterial oxidation of nicotinic acid. *J. Biol. Chem. 228* (2), 923−945.

(12) Alhapel, A., Darley, D. J., Wagener, N., Eckel, E., Elsner, N., and Pierik, A. J. (2006) Molecular and functional analysis of nicotinate catabolism in *Eubacterium barkeri*. *Proc. Natl. Acad. Sci. U. S. A. 103* (33), 12341−12346.

(13) Huijbers, M. M. E., Montersino, S., Westphal, A. H., Tischler, D., and van Berkel, W. J. H. (2014) Flavin dependent monooxygenases. *Arch. Biochem. Biophys. 544* (0), 2−17.

(14) Ballou, D. P., and Entsch, B. (2013) In Handbook of Flavoproteins: Complex Flavoproteins. *Dehydrogenases and Physical Methods 2*, 1−28.

(15) Montersino, S., Tischler, D., Gassner, G. T., and Van Berkel, W. J. H. (2011) Catalytic and structural features of flavoprotein hydroxylases and epoxidases. *Adv. Synth. Catal. 353*, 2301−2319.

(16) Hicks, K. A., Yuen, M. E., Zhen, W. F., Gerwig, T. J., Story, R. W., Kopp, M. C., and Snider, M. J. (2016) Structural and biochemical

DOI: 10.1021/acs.biochem.8b00969
Biochemistry 2019, 58, 1751−1763

characterization of 6-hydroxynicotinic acid 3-monooxygenase, a novel decarboxylative hydroxylase involved in aerobic nicotinate degradation. *Biochemistry 55* (24), 3432−3446.
(17) Palfey, B. A., Moran, G. R., Entsch, B., Ballou, D. P., and Massey, V. (1999) Substrate recognition by "password" in *p*-hydroxybenzoate hydroxylase. *Biochemistry 38* (4), 1153−1158.
(18) Eppink, M. H., Boeren, S. A., Vervoort, J., and van Berkel, W. J. (1997) Purification and properties of 4-hydroxybenzoate 1-hydroxylase (decarboxylating), a novel flavin adenine dinucleotide-dependent monooxygenase from *Candida parapsilosis* CBS604. *J. Bacteriol. 179* (21), 6680−6687.
(19) Husain, M., Entsch, B., Ballou, D. P., Massey, V., and Chapman, P. J. (1980) Fluoride elimination from substrates in hydroxylation reactions catalyzed by *p*-hydroxybenzoate hydroxlyase. *J. Biol. Chem. 255* (9), 4189−4197.
(20) Mascotti, M. L., Juri Ayub, M., Furnham, N., Thornton, J. M., and Laskowski, R. A. (2016) Chopping and changing: the evolution of flavin-dependent monooxygenases. *J. Mol. Biol. 428* (15), 3131−3146.
(21) Qiu, J., Liu, B., Zhao, L., Zhang, Y., Cheng, D., Yan, X., Jiang, J., Hong, Q., and He, J. (2018) A novel degradation mechanism for pyridine derivatives in *Alcaligenes faelcalis* JQ135. *Appl. Environ. Microbiol. 84* (15), e00910−18.
(22) Yu, H., Hausinger, R. P., Tang, H. Z., and Xu, P. (2014) Mechanism of the 6-hydroxy-3-succinoyl-pyridine 3-monooxygenase flavoprotein from *Pseudomonas putida* S16. *J. Biol. Chem. 289* (42), 29158−29170.
(23) Nakano, H., Wieser, M., Hurh, B., Kawai, T., Yoshida, T., Yamane, T., and Nagasawa, T. (1999) Purification, characterization and gene cloning of 6-hydroxynicotinate 3-monooxygenase from Pseudomonas fluorescens TN5. *Eur. J. Biochem. 260* (1), 120−126.
(24) Nichol, G. S., and Clegg, W. (2005) 6-Methyl-2-pyridone: an elusive structure finally solved. *Acta Crystallogr., Sect. C: Cryst. Struct. Commun. 61*, o383−o385.
(25) van Berkel, W. J. H., and Muller, F. (1989) The temperature and pH dependence of some properties of *p*-hydroxybenzoate hydroxylase from *Pseudomonas fluorescens*. *Eur. J. Biochem. 179*, 307−314.
(26) Friesner, R. A., Murphy, R. B., Repasky, M. P., Frye, L. L., Greenwood, J. R., Halgren, T. A., Sanschagrin, P. C., and Mainz, D. T. (2006) Extra Precision Glide: Docking and Scoring Incorporating a Model of Hydrophobic Enclosure for Protein−Ligand Complexes. *J. Med. Chem. 49* (21), 6177−6196.
(27) Montersino, S., Orru, R., Barendregt, A., Westphal, A. H., van Duijn, E., Mattevi, A., and van Berkel, W. J. H. (2013) Crystal structure of 3-hydroxybenzoate 6-hydroxylase uncovers lipid-assisted flavoprotein strategy for regioselective aromatic hydroxylation. *J. Biol. Chem. 288* (36), 26235−26245.
(28) Sucharitakul, J., Medhanavyn, D., Pakotiprapha, D., van Berkel, W. J. H., and Chaiyen, P. (2016) Tyr217 and His213 are important for substrate binding and hydroxlyation of 3-hydroxybenzoate 6-hydroxylase from *Rhodococcus jostii RHA1*. *FEBS J. 283*, 860−881.
(29) Treiber, N., and Schulz, G. E. (2008) Structure of 2,6-dihydroxypyridine 3-hydroxylase from a nicotine-degrading pathway. *J. Mol. Biol. 379* (1), 94−104.
(30) Uemura, T., Kita, A., Watanabe, Y., Adachi, M., Kuroki, R., and Morimoto, Y. (2016) The catalytic mechanism of decarboxylative hydroxylation of salicylate hydroxylase revealed by crystal structure analysis at 2.5 Å resolution. *Biochem. Biophys. Res. Commun. 469* (2), 158−163.
(31) Hiromoto, T., Fujiwara, S., Hosokawa, K., and Yamaguchi, H. (2006) Crystal structure of 3-hydroxybenzoate hydroxylase from *Comamonas testosteroni* has a large tunnel for substrate and oxygen access to the active site. *J. Mol. Biol. 364*, 878−896.
(32) Gatti, D. L., Entsch, B., Ballou, D. P., and Ludwig, M. L. (1996) pH-Dependent Structural Changes in the Active Site of *p*-Hydroxybenzoate Hydroxylase Point to the Importance of Proton and Water Movements during Catalysis. *Biochemistry 35* (2), 567−578.
(33) Ortiz-Maldonado, M., Entsch, B., and Ballou, D. P. (2004) Oxygen Reactions in *p*-Hydroxybenzoate Hydroxylase Utilize the H-Bond Network during Catalysis. *Biochemistry 43*, 15246−15257.
(34) Eschrich, K., van der Bolt, F. J. T., de Kok, A., and van Berkel, W. J. H. (1993) Role of Tyr201 and Tyr385 in substrate activation by p-hydroxybenzoate hydroxylase from Pseudomonas fluorescens. *Eur. J. Biochem. 216*, 137−146.
(35) McCulloch, K. M., Mukherjee, T., Begley, T. P., and Ealick, S. E. (2009) Structure of the PLP Degradative Enzyme 2-Methyl-3-hydroxypyridine-5-carboxylic Acid Oxygenase from *Mesorhizobium loti* MAFF303099 and Its Mechanistic Implications. *Biochemistry 48* (19), 4139−4149.
(36) Hicks, K. A., O'Leary, S. E., Begley, T. P., and Ealick, S. E. (2013) Structural and Mechanistic Studies of HpxO, a Novel Flavin Adenine Dinucleotide-Dependent Urate Oxidase from *Klebsiella pneumoniae*. *Biochemistry 52* (3), 477−487.

DOI: 10.1021/acs.biochem.8b00969
Biochemistry 2019, 58, 1751−1763